Dynamics of DNA in the Flow−Gradient Plane of Steady Shear Flow: Observations and Simulations

ARTICLE *in* MACROMOLECULES · FEBRUARY 2005

Impact Factor: 5.8 · DOI: 10.1021/ma0480796

4 AUTHORS, INCLUDING:

Eric S. G. Shaqfeh
Stanford University
221 PUBLICATIONS **5,764** CITATIONS

Dynamics of DNA in the Flow-Gradient Plane of Steady Shear Flow: Observations and Simulations

Charles M. Schroeder,[†] Rodrigo E. Teixeira,[†] Eric S. G. Shaqfeh,[*,‡] and Steven Chu[§]

Department of Chemical Engineering, Stanford University, Stanford, California 94305; Departments of Chemical and Mechanical Engineering, Stanford University, Stanford, California 94305; and Departments of Physics and Applied Physics, Stanford University, Stanford, California 94305

Received September 16, 2004; Revised Manuscript Received November 15, 2004

ABSTRACT: The dynamical behavior of DNA in steady shear flow has been elucidated using a combination of Brownian dynamics (BD) simulation and single molecule visualization using fluorescence microscopy. Observations of DNA motion in the flow-gradient plane of shear flow using a novel flow apparatus allow for measurement of the gradient-direction polymer thickness (δ_2), a microscopic conformational property that has direct influence on macroscopic polymer solution properties. To complement experimental results for λ-phage DNA (22 μm in length) and 84 μm DNA, we present BD simulation results for DNA in terms of both free-draining bead−spring models and models including both intramolecular hydrodynamic interactions (HI) and excluded volume (EV) interactions. Good agreement between experiments and BD simulations is obtained for ensemble averaged measurements of polymer extension, δ_2, and orientation angle over a wide range of flow strengths. Macroscopic solution properties, including the polymer contribution to the shear viscosity (η^p) and first normal stress coefficient (Ψ_1^p), are calculated in BD simulations. Power law scalings of η^p and Ψ_1^p from the single molecule experiment and BD simulation agree well with bulk rheological characterization of dilute polymer solutions. Histograms of polymer extension demonstrate good agreement between experiment and BD simulation, though histograms of δ_2 from BD simulation slightly differ from experimental results. Cross-correlations of polymer extension and δ_2 display rich dynamical polymer behavior, which we discuss on a physical basis. Finally, the power spectral density of polymer extension and δ_2 is presented for DNA for both single molecule experiment and BD simulation.

1. Introduction

The dynamical behavior of flexible polymer molecules in simple shear flow is replete with interesting and complex physics.[1−3] Fluid flow past any solid boundary gives rise to shear flow.[4] The ubiquitous nature of this flow type engenders a great deal of practical interest. Dilute solutions of flexible polymers in shear flow exhibit flow-dependent viscosities and enhanced normal stresses.[1] These macroscopically observed quantities arise from microscopic, flow-induced conformational changes in polymer chains.

Flow type directly influences the nature of the conformational response of a polymer.[5,6] In general, a two-dimensional, planar flow may be created from a linear superposition of varying amounts of purely extensional and purely rotational flow.[4] Extension dominated flows such as those produced in injection molding applications or near the stagnation point in cross-slot devices are very effective in stretching flexible polymer molecules.[1,3,7] Fluid flows with dominant amounts of rotation tend not to perturb polymer conformations far from the coiled state.[3,6] Simple shear flow consists of equal amounts of rotation and extension giving rise to intriguing, albeit complicated, polymer physics. It is now known that in simple shear flow flexible polymers never reach a steady-state molecular extension;[8] rather, individual polymer chains continually undergo tumbling motion with large fluctuations in polymer extension.[8,9] Results from earlier computational studies of Liu[10] and Doyle et al.[11] support this experimental observation.

A primary goal of polymer rheology is to establish a direct link between microscopic quantities such as polymer conformation and macroscopic experimental quantities such as solution viscosity. Traditional experiments involving optical techniques such as birefringence and light and neutron scattering have sought polymer microstructural information in shear flow.[12−17] Light scattered by flowing macromolecules may be used to infer conformational information through the radius of gyration tensor.[15] Many experiments employing light scattering techniques indicated that polymers did not substantially stretch in shear.[15,17] Although the flow strengths probed were generally low due to technical issues, experimentally determined polymer conformation changes were considerably smaller than predicted by Rouse and Zimm models for polymer dynamics or by Brownian dynamics simulations of nonlinear bead−spring chains.[17]

Single molecule techniques using fluorescence microscopy have allowed for the direct observation of DNA chains in flowing solution[7,8,18−20] The first single molecule study of fluorescent DNA in simple shear flow showed that polymers may indeed substantially stretch in shear flow.[8] Furthermore, observation of DNA dynamics in steady shear revealed large fluctuations in polymer extension, suggestive of end-over-end polymer tumbling. Observations from the experimental study of Smith et al.[8] showed that although DNA molecules constantly exhibit large (atemporal) fluctuations in molecular extension, the average polymer extension

[†] Department of Chemical Engineering.
[‡] Departments of Chemical and Mechanical Engineering.
[§] Departments of Physics and Applied Physics.
* To whom correspondence should be addressed. E-mail: eric@chemeng.stanford.edu.

10.1021/ma0480796 CCC: $30.25
Published on Web 02/10/2005

asymptotes to a value approximately one-half of the contour length at high flow strengths. In another study, Babcock et al.[21] examined the relationship between the transient solution viscosity measured using bulk shear rheology and polymer conformation during the onset of shear flow. In this work, the authors relate the overshoot in the transient shear viscosity to nonaffine polymer motion using a combination of single molecule fluorescence microscopy and Brownian dynamics simulation.

In addition to experimental studies, the dynamics of flexible polymers in simple shear flow has also been examined using theory- and simulation-based approaches. Polymer kinetic theory may be used to derive equations for the moments of polymer chain extension, and knowledge of the flow-induced conformations may be used to calculate rheological functions such as shear viscosity. Results from polymer kinetic theory for a Hookean dumbbell show a constant shear viscosity as a function of flow strength and hence no shear thinning.[2,22] Inclusion of a nonlinear entropic spring (such as the Warner spring, an analytic approximation to the inverse Langevin function for synthetic polymers) leads to calculation of a shear-thinning polymer viscosity and first normal stress coefficient with the preaveraging approximation.[2,22,23] Interestingly, inclusion of intramolecular hydrodynamic interactions into the equations of motion for a Hookean dumbbell model solved using a consistently averaged or Gaussian approximation yields a shear-thinning viscosity in weak shear flow.[22,24]

More recently, research investigations using Brownian dynamics (BD) simulation of bead−rod or bead−spring polymer models have elucidated the nonlinear behavior of polymer chains in flow and proven the utility of studying stochastic models in polymer physics. With regard to free-draining polymer models, Liu[10] used BD simulations to probe the rheological behavior of Kramers freely jointed bead−rod phantom chains in steady shear flow. For bead−rod chains containing up to 20 beads, Liu found shear thinning exponents of −1/2 and −4/3 for the steady shear viscosity and first normal stress coefficient, respectively. Doyle et al.[11] also used BD simulation to investigate the dynamical behavior of polymers in steady shear flow and calculated rheological properties such as shear viscosity and normal stress differences, and in addition, polymer conformational properties such as extinction angle. BD simulation was used by Hur et al.[25] to study the dynamical behavior of λ-phage DNA in steady shear flow with a free-draining polymer model. Good agreement between results obtained from simulation and experiment in terms of average polymer extension was shown for bead−rod chains and for multimode bead−spring chains using the appropriate nonlinear (Marko−Siggia) force law for double-stranded DNA.[26] Furthermore, the flow strength dependence of the gradient direction DNA thickness (δ_2) from BD simulation agrees well with a Graetz−Levecque scaling argument based on a coupling between chain advection in the flow direction and transverse chain diffusion in the gradient direction.[11]

In addition to the steady shear dynamics of DNA, the transient polymer response has also been studied using BD simulation and fluorescence microscopy. In another paper, Hur et al.[27] studied the transient behavior of λ-DNA molecules in the start-up of shear flow. Again, good agreement between average polymer extension from BD simulation of free-draining polymer chains and single molecule experiment is shown. The authors compare the polymer contribution to the shear viscosity (η^p) in dilute solution simulations to experimentally measured shear viscosities. Experimental measurements of η^p were made using bulk rheology of λ-DNA solutions with concentrations up to $6c^*$, where c^* is the polymer overlap concentration. Interestingly, BD simulations of dilute solutions of DNA agree well with experimentally measured η^p when the polymer relaxation time in simulation is accurately adjusted to reflect semidilute solution behavior.

Additional studies have focused on the effect of hydrodynamic interactions (HI) on polymer dynamics in shear flow using BD simulation.[28−31] De la Torre and co-workers have presented a series of BD simulations for polymer models with the inclusion of nonpreaveraged hydrodynamic interactions.[32−34] Recently, Cifre and de la Torre[35] investigated the polymer orientation behavior with BD simulations of a bead−spring polymer model with HI and excluded volume (EV) interactions in dilute solutions in shear flow. Jendrejack et al.[31] demonstrated that inclusion of intramolecular HI does not quantitatively change the average steady-state extension of λ-DNA in shear flow. Furthermore, results from Jendrejack et al.[31] showed essentially no difference between free-draining and HI models with respect to the shear-thinning exponents for viscosity and first normal stress coefficient for 84 μm ($\approx 4\lambda$) DNA. Similarly, simulations of λ-DNA in extensional flow reveal that the dynamics do not quantitatively change upon inclusion of intramolecular HI for bead−spring polymer models.[31,36] However, the role of intramolecular HI becomes increasingly important for larger DNA and leads to dramatic effects on the coil−stretch transition in planar extensional flow.[20,37]

Recently, Teixeira et al.[9] directly observed DNA dynamics in the flow-gradient plane of simple shear using a novel flow device. In this work, the authors directly measured the polymer configuration thickness (δ_2) in the gradient direction of shear flow. Solution viscosity is directly related to δ_2, a microscopic conformational polymer property. Therefore, this experimental study establishes a link between microscopic polymer quantities and macroscopic solution properties in dilute solutions. A detailed description of the polymer tumbling mechanism is presented, and scaling arguments describing the dynamical end-over-end polymer motion are discussed.

The goal of the present work is to directly compare results from Brownian dynamics simulations of flexible DNA molecules to recently measured flow-gradient plane DNA properties in simple shear flow. To this end, we present additional experimental data for 84 μm DNA in shear flow. For BD simulations, we model DNA molecules as bead−spring polymer chains and compare simulation results for free-draining (FD) molecules and for chains with intramolecular hydrodynamic interactions with interbead excluded volume interactions (EV).[37]

2. Experimental Section

Fluorescent DNA molecules were imaged in the flow-gradient plane of simple shear flow using a novel apparatus. The device and methods are described at length in a companion article.[9] In short, simple shear flow was generated between two parallel, optically transparent quartz microscope slides translating in opposite directions. A thin mica sheet was placed

between the quartz slides, providing a well-maintained gap (h) of approximately 34 μm. Two feedback-controlled motors (Oriel) were used in the apparatus: one motor translated the shear surface at a constant speed (v) while the second motor moved the flow assembly in the opposite direction. By carefully adjusting the speed of the assembly translation, we are able to observe a single fluorescent DNA molecule for several hundred strain units (γ). Accumulated fluid strain is defined by the relation $\gamma = \dot{\gamma}t$, where $\dot{\gamma} = v/h$ is the shear rate and t is the observation time. Light emitted from fluorescent DNA molecules in the small gap passed through the shearing walls and through a thin coverslip before being collected by the microscope objective lens. To minimize distortions of the DNA images, we match the index of refraction (n) of the shearing walls to the solution by adjusting the sucrose concentration to 67.1% (w/w). The solution viscosity was 300 cP, and the index of refraction was matched to $n = 1.458$. Experiments were conducted at 17 °C.

An inverted, home-built microscope equipped for epifluorescence was used to image DNA. A back-illuminated Micromax 512BFT CCD camera (Roper Scientific) provided images of fluorescent DNA. We observed the dynamics of λ-DNA (48.5 kbp, Gibco BRL, 22 μm stained contour length) and $\approx$84 μm DNA (185 kbp, a generous gift from US Genomics). A 5% error is attributed to estimation of the contour length of 84 μm DNA based on pulsed field gel electrophoresis studies. DNA was stained with YOYO-1 fluorescent dye (Molecular Probes) and imaged in solution buffers as described in previous work.[8,37]

3. General Procedures

In this work, we studied the dynamics of polymers in simple shear flow. The flow, shear gradient, and vorticity directions are defined as the "1", "2", and "3" directions, respectively. The flow field is then described by

$$u_i(x_2) = \dot{\gamma} x_2 \delta_{i1}; \quad \frac{\partial u_i}{\partial x_j} = \dot{\gamma}\delta_{i1}\delta_{j2} \tag{1}$$

where u_i is the fluid velocity, $\partial u_i/\partial x_j$ is the velocity gradient tensor, and δ_{ij} is the second-order isotropic tensor. In eq 1, subscripts refer to tensorial indices. Polymer relaxation times were measured by first stretching DNA molecules at high shear rates, followed by tracking polymer projected images over time after cessation of flow. Relaxation times were calculated by fitting the final 30% of the polymer extension (x) to a decaying exponential function $\langle x \cdot x \rangle = A \exp(-t/\tau) + B$, where τ is the longest polymer relaxation time, t is observation time, and A and B are fitting constants. The relaxation times for λ-DNA and 84 μm DNA in the 300 cP sucrose solution were 28 and 251 s, respectively. A dimensionless shear rate, the Weissenberg number ($Wi = \dot{\gamma}\tau$), is defined as the ratio of the polymer relaxation time to the characteristic flow time scale ($\dot{\gamma}^{-1}$). Finally, we tracked the steady shear dynamics of single DNA molecules over the course of many strain units, generally ignoring the transient (start-up) polymer behavior during the first $\approx$70 strain units in experiment[27] and $\approx$500 strain units in BD simulation.

Movies of DNA dynamics were analyzed to extract the maximum projected chain extension in the flow direction and the radius of gyration tensor. Note that the projected extension is not, in general, equal to the polymer end-to-end distance, as the chain ends are not easily resolved with our optical setup. The radius of gyration tensor is defined as

$$G_{ij} \equiv \frac{\sum_{p,q} I(p,q) R_i^{p,q} R_j^{p,q}}{\sum_{p,q} I(p,q)} \tag{2}$$

where $I(p,q)$ gives the intensity of the polymer image at the pth column, qth row pixel, accurately corrected to subtract the background level, and $R_i^{p,q}$ is the two-dimensional vector from the polymer center-of-mass to the pth column and qth row pixel. The elements of the radius of gyration tensor accessible with our experimental setup are G_{11}, G_{22}, and $G_{12} = G_{21}$.

In bead−rod or bead−spring polymer models, the radius of gyration tensor for a chain composed of N beads is given by[23]

$$G_{ij} = \frac{1}{N}\sum_{\nu=1}^{N} R_i^{\nu} R_j^{\nu} \tag{3}$$

where R_i^{ν} is the position of bead ν with respect to the chain center-of-mass. The experimental measurement of G_{ij} is equivalent to the definition for G_{ij} given in eq 3 within our assumption that image intensity is linearly related to polymer mass at a particular image location. This assumption is justified because staining DNA with the fluorescent dye YOYO-1 is insensitive to base pair sequence (at least within the resolution limit of the microscope, $\approx$0.3 μm). Furthermore, the entire DNA molecule is maintained in the image plane of the microscope corresponding to the two-dimensional shear flow plane. Finally, our CCD camera is nonintensified, allowing for a linear relationship between the intensity of light impinging on a pixel and the final value of the digital intensity in the acquired image.

Using the definition of G_{ij} given by eq 2 for experiments and eq 3 for Brownian dynamics simulations, two additional quantities may be calculated. The polymer thickness in the gradient direction (δ_2) is defined as

$$\delta_2 = \sqrt{G_{22}} \tag{4}$$

In addition, the polymer orientation angle (θ) relative to the flow direction is given by

$$\tan(2\theta) = \frac{2G_{12}}{G_{11} - G_{22}} \tag{5}$$

Orientation angles are defined to be positive when measured from the flow ("1") axis toward the gradient ("2") axis in the flow-gradient plane.

It is often convenient to characterize the time and frequency dependence of fluctuating quantities by observing the power of a signal in Fourier space. The power spectral density (PSD) is defined as the Fourier transform of the autocorrelation of a quantity (or cross-correlation of two quantities).[8,25,38] The autocorrelation of a real valued, fluctuating quantity $x(t)$ is given by

$$C_{x,x}(T) = \langle x(t)\, x(t+T) \rangle \tag{6}$$

where brackets denote a time-averaged quantity, t is

time, and T is an offset time. The PSD of a stationary stochastic process is

$$P(f) = \int_{-\infty}^{\infty} C_{x,x}(T) e^{-2i\pi fT} \, dT \tag{7}$$

where f is frequency and $i = \sqrt{-1}$. In calculation of PSDs given by eq 7, we first subtract the mean value from each data point in a time series of a (stationary) fluctuating quantity. We then use fast Fourier transform (FFT)[38] algorithm to find the PSD of a quantity. PSDs are normalized by the total length of a stretch of transformed data. In calculation of the PSD of polymer extension, power is made dimensionless by the quantity $R_g^2\tau$.[8] Finally, frequency is nondimensionalized by the longest polymer relaxation time τ.

4. Brownian Dynamics Simulation

4.1. Model Description. We employ a model for Brownian dynamics simulation of a system of N particles that are subject to interparticle forces and fluctuating hydrodynamic interactions as originally presented by Ermak and McCammon.[39] This model is used in a bead−spring description of flexible polymer molecules in dilute solution flows and was presented in detail in previous work.[37] A statement of force balance for each bead i yields the Langevin equations for a system of N Brownian particles with interparticle forces and fluctuating HI. The Langevin equations may be manipulated to yield set of a stochastic differential equations for the positions of beads $i = 1$ to N:[39]

$$d\mathbf{r}_i = \left(\kappa \cdot \mathbf{r}_i + \sum_{j=1}^{N} \frac{\partial}{\partial \mathbf{r}_j} \cdot \mathbf{D}_{ij} + \sum_{j=1}^{N} \frac{\mathbf{D}_{ij} \cdot \mathbf{F}_j}{kT} \right) dt + \sqrt{2} \sum_{j=1}^{i} \boldsymbol{\alpha}_{ij} \cdot d\mathbf{W}_j \tag{8}$$

where $\mathbf{r}_i$ is the position of bead i, $\mathbf{D}_{ij}$ is the mobility tensor, $\mathbf{F}_i$ is the net interparticle (entropic spring and excluded volume) force on bead i, and $d\mathbf{W}_j$ is a Wiener process[2] that may be described by the relation $d\mathbf{W}_j = \sqrt{dt}\,\mathbf{n}_j$. The quantity $\mathbf{n}_j$ is a randomly distributed Gaussian vector with zero mean and unit variance. In eq 8, $\mathbf{D}_{ij}$ is related to the coefficient tensor $\boldsymbol{\alpha}_{ij}$ by the relation:

$$\mathbf{D}_{ij} = \sum_{l=1}^{N} \boldsymbol{\alpha}_{il} \cdot \boldsymbol{\alpha}_{jl} \tag{9}$$

We assume a spatially homogeneous velocity field such that the solvent velocity $\mathbf{v}(\mathbf{r})$ can be expressed as $\mathbf{v}(\mathbf{r}) = \kappa \cdot \mathbf{r}$, where κ is the (constant) velocity gradient tensor. For simple shear flow, the velocity gradient tensor is given by

$$\kappa = \begin{pmatrix} 0 & \dot{\gamma} & 0 \\ 0 & 0 & 0 \\ 0 & 0 & 0 \end{pmatrix} \tag{10}$$

We choose $\mathbf{D}_{ij}$ as the Rotne−Prager−Yamakawa (RPY) tensor,[41] which has been proven to be positive-semidefinite for all polymer chain configurations. The RPY tensor has the added advantage that terms in eq 8 involving its spatial gradients are exactly zero; this feature greatly simplifies computations. The RPY mobility tensor is given by

$$\mathbf{D}_{ij} = \frac{kT}{\zeta} \mathbf{I}_{ij} \quad \text{if } i = j \tag{11}$$

$$\mathbf{D}_{ij} = \frac{kT}{8\pi\eta r_{ij}} \left[\left(1 + \frac{2a^2}{3r_{ij}^2} \right) \mathbf{I}_{ij} + \left(1 - \frac{2a^2}{r_{ij}^2} \right) \frac{\mathbf{r}_{ij}\mathbf{r}_{ij}}{r_{ij}^2} \right] \quad \text{if } i \neq j \text{ and } r_{ij} \geq 2a \tag{12}$$

$$\mathbf{D}_{ij} = \frac{kT}{\zeta} \left[\left(1 - \frac{9r_{ij}}{32a} \right) \mathbf{I}_{ij} + \frac{3\mathbf{r}_{ij}\mathbf{r}_{ij}}{32a r_{ij}} \right] \quad \text{if } i \neq j \text{ and } r_{ij} < 2a \tag{13}$$

where a is the bead radius, $\mathbf{r}_{ij}$ is the vector between beads i and j, ζ is the bead resistivity, and $r_{ij} = |\mathbf{r}_{ij}|$. The quantity h^* is often defined as the hydrodynamic interaction parameter in HI studies such that

$$h^* = a\sqrt{\frac{H}{\pi kT}} \tag{14}$$

The Hookean spring constant H is given by $H = 3kT/N_{k,s}b_k^2$. The quantity h^* in eq 14 is the approximate ratio of the bead radius to the equilibrium extension of a spring; we therefore anticipate physically reasonable values of h^* to be $\lesssim 1/2$.[2] It should be noted that the quantity h^* arises naturally as a collection of constants that appears in an expression for the preaveraged Oseen tensor. Therefore, h^* and the bead radius a are related quantities and should not be chosen separately.

Equation 8 is nondimensionalized with an appropriate length scale (l_s) and time scale (t_s) such that $t_s = \zeta/4H$ and $l_s = \sqrt{kT/H}$,[42] where ζ is the bead resistivity. In this model, each spring is finitely extensible and represents only a portion of the entire polymer molecule, where the number of Kuhn steps per spring is denoted as $N_{k,s}$. The total number of Kuhn segments $N_{k,tot}$ in the molecule is $N_{k,tot} = (N - 1)N_{k,s}$, the Kuhn step size is b_k, and the total dimensional contour length L of the macromolecule is $L = N_{k,tot}b_k$. The spring connector vector for spring i can be defined as $\mathbf{Q}_i = \mathbf{r}_{i+1} - \mathbf{r}_i$. We now recast the eq 8 in terms of the spring connector vectors in dimensionless form as

$$d\mathbf{Q}_i = [Pe(\kappa \cdot \mathbf{Q}_i) + \sum_{j=1}^{N} (\mathbf{D}_{i+1,j} - \mathbf{D}_{i,j}) \cdot (\mathbf{F}_j^{E} + \mathbf{F}_j^{EV})] \, dt + \sqrt{2} \sum_{j=1}^{i+1} (\boldsymbol{\alpha}_{i+1,j} - \boldsymbol{\alpha}_{i,j}) \cdot d\mathbf{W}_j \tag{15}$$

where the subscripts on vector $\mathbf{Q}$ refer to spring vectors such that $1 \leq i \leq N - 1$, $\mathbf{F}_i^{E}$ is the net entropic spring force exerted on bead i, $\mathbf{F}_i^{EV}$ is the net excluded volume force on bead i, and Pe is the bead Péclet number such that $Pe = \dot{\gamma}\zeta/4H$. The total entropic force on bead i is given by

$$\mathbf{F}_i^{E} = \begin{cases} \mathbf{F}_1^{s} & \text{if } i = 1 \\ \mathbf{F}_i^{s} - \mathbf{F}_{i-1}^{s} & \text{if } 1 < i < N \\ -\mathbf{F}_{N-1}^{s} & \text{if } i = N \end{cases} \tag{16}$$

where subscripts on the right-hand side of eq 16 refer to spring indices. We use the Marko−Siggia[26] expression for the restoring force of an entropic "wormlike" spring

between two beads in the bead−spring chain:

$$\mathbf{F}_i^s = \frac{kT}{b_k}\left[\frac{1}{2}\frac{1}{\left(1-\frac{Q}{Q_0}\right)^2} - \frac{1}{2} + \frac{2Q}{Q_0}\right]\frac{\mathbf{Q}_i}{Q} \tag{17}$$

where Q_0 is the maximum extensibility of a spring such that $Q_0 = N_{k,s}b_k$, and Q is the scalar magnitude of the spring extension vector $\mathbf{Q}_i$ for spring i. Equation 17 gives the wormlike chain (WLC) restoring force appropriate for double-stranded DNA.

Excluded volume (EV) interactions are incorporated into our bead−spring model for polymer chains to accurately capture good solvent behavior of DNA in aqueous solution. EV effects are modeled as short-range interactions that directly affect chain dynamics when two polymer segments (beads) come into close approach. The energy of interaction between beads i and j in a bead−spring chain can be expressed as[31]

$$U_{ij}^{EV} = \frac{1}{2}\nu kTN_{k,s}{}^2\left(\frac{3}{4\pi R_{g,sub}{}^2}\right)^{3/2}\exp\left[-\frac{3r_{ij}{}^2}{4R_{g,sub}{}^2}\right] \tag{18}$$

where the vector between beads i and j is defined as $\mathbf{r}_{ij} = \mathbf{r}_j - \mathbf{r}_i$, $|\mathbf{r}_{ij}| = r_{ij}$, ν is the excluded volume coefficient, and $R_{g,\,sub} = \sqrt{N_{k,s}b_k{}^2/6}$ is the radius of gyration of a subsection of the polymer chain. Specifically, we employ this expression for the potential proposed by Jendrejack et al.[31] because it contains an explicit dependence on chain discretization. After taking the gradient of the potential and scaling by appropriate quantities, we arrive at an expression for the dimensionless EV force on bead i:

$$\mathbf{F}_i^{EV} = -\sum_{j=1;i\neq j}^{N}\sqrt{3}z\left(\frac{9}{2}\right)\exp\left[-\frac{3r_{ij}{}^2}{2}\right]\mathbf{r}_{ij} \tag{19}$$

where $z = (1/2\pi)^{3/2}\tilde{\nu}N_{k,s}{}^2$. The quantity z is related to a common perturbation parameter for EV interactions in analytic theories[43] and is defined here in terms of a dimensionless EV parameter $\tilde{\nu}$. A more complete discussion regarding the choice of EV interactions may be found elsewhere.[37]

A highly efficient predictor−corrector algorithm is used to solve the set of eqs 15 for the spring connector vectors at each time step. This algorithm was originally proposed for general free-draining bead−spring chains.[42] Recently, it was extended to model polymers with fluctuating HI[36] and shown to be significantly more efficient than either explicit Euler or iterative Newton solution schemes. In this and previous work,[37] we modify the original model as described by Somasi et al.[42] to include both fluctuating intrachain HI *and* excluded volume interactions. Finally, Cholesky's method was used to decompose the diffusivity tensor $\mathbf{D}_{ij}$ at the beginning of each time step to calculate $\boldsymbol{\alpha}_{ij}$. A detailed description of the model algorithm may be found in Schroeder et al.[37]

4.2. Calculation of Polymer Stress. The total stress in a solution of flexible polymers ($\boldsymbol{\tau}^{tot}$) is given by[23]

$$\boldsymbol{\tau}^{tot} = \boldsymbol{\tau}^s + \boldsymbol{\tau}^p - P\boldsymbol{\delta} \tag{20}$$

where $\boldsymbol{\tau}^s$ is the deviatoric solution stress arising from the Newtownian solvent:

$$\boldsymbol{\tau}^s = \eta^s(\nabla\mathbf{u} + (\nabla\mathbf{u})^\dagger) \tag{21}$$

where η^s is the solvent viscosity and $\mathbf{u}$ is the velocity. In eq 20, P is the isotropic solution pressure and acts normal to all surfaces. The transpose of a tensor $\mathbf{A}$ is denoted as $\mathbf{A}^\dagger$. Finally, $\boldsymbol{\tau}^p$ is the polymer contribution to the stress. For bead−spring chains with intramolecular HI and excluded volume interactions, the Kramers form of the stress tensor is used to calculate the polymer contribution to the total stress:[23]

$$\boldsymbol{\tau}^p = n\sum_{k=1}^{N_s}\langle\mathbf{Q}_k\mathbf{F}_k^s\rangle - n\sum_{\nu=1}^{N}\sum_{k=1}^{N_s}B_{\nu k}\langle\mathbf{Q}_k\mathbf{F}_\nu^{EV}\rangle - N_s(nkT)\boldsymbol{\delta} \tag{22}$$

where $N_s = (N-1)$ is the number of springs, n is the number concentration of polymers in solution, kT is the thermal energy, and $\mathbf{B}$ is a matrix defined by the relation

$$B_{\nu k} = \begin{cases}\dfrac{k}{N} & \text{if } k < \nu \\ -\left(1-\dfrac{k}{N}\right) & \text{if } k \geq \nu\end{cases} \tag{23}$$

Stress is made dimensionless with the quantity nkT, and the nondimensional form of eq 22 becomes

$$\boldsymbol{\tau}^p = \sum_{k=1}^{N_s}\langle\mathbf{Q}_k\mathbf{F}_k^s\rangle - \sum_{\nu=1}^{N}\sum_{k=1}^{N_s}B_{\nu k}\langle\mathbf{Q}_k\mathbf{F}_\nu^{EV}\rangle - N_s\boldsymbol{\delta} \tag{24}$$

For free-draining bead−spring chains, the Giesekus form of the stress tensor may be used to calculate the polymer contribution to the total stress.[11,23] In dimensionless form, the Giesekus stress tensor is

$$\boldsymbol{\tau}^p = -2\frac{\mathscr{D}}{\mathscr{D}t}\sum_{\nu=1}^{N}\langle\mathbf{R}^\nu\mathbf{R}^\nu\rangle \tag{25}$$

where $\mathscr{D}/\mathscr{D}t$ denotes a convected time derivative such that[23]

$$\frac{\mathscr{D}}{\mathscr{D}t}\mathbf{A} = \frac{\mathrm{d}}{\mathrm{d}t}\mathbf{A} - (\boldsymbol{\kappa}\cdot\mathbf{A} + \mathbf{A}\cdot\boldsymbol{\kappa}^\dagger) \tag{26}$$

where $\mathbf{A}$ is a second-order tensor. At steady state, eq 25 simplifies to

$$\boldsymbol{\tau}^{p,ss} = 2\sum_{\nu=1}^{N}\langle\boldsymbol{\kappa}\cdot\mathbf{R}^\nu\mathbf{R}^\nu + \mathbf{R}^\nu\mathbf{R}^\nu\cdot\boldsymbol{\kappa}^\dagger\rangle \tag{27}$$

In dimensionless form, the polymer contribution to the shear viscosity is defined as

$$\eta^p = \frac{\tau_{12}^p}{Pe} \tag{28}$$

Finally, the dimensionless first normal stress coefficient is given by

$$\Psi_1^p = \frac{(\tau_{11}^p - \tau_{22}^p)}{Pe^2} \tag{29}$$

Using the expression for the Giesekus stress tensor in eq 27 at steady state, the polymer contribution to the shear viscosity becomes[11]

$$\eta^{p,ss} = 2\sum_{\nu=1}^{N}\langle R_2^\nu R_2^\nu\rangle \tag{30}$$

and the first normal stress coefficient becomes

$$\Psi_1^{p,ss} = \frac{4}{Pe}\sum_{\nu=1}^{N}\langle R_1^\nu R_2^\nu\rangle \tag{31}$$

It is immediately obvious that the polymer contribution to the shear viscosity η^p scales linearly with G_{22} such that $\eta^p \sim G_{22}$ (hence $\eta_p \sim \delta_2{}^2$), and the first normal stress coefficient scales as $\Psi_1^p \sim G_{12}/Pe$. Although eqs 30 and 31 *apply only to free-draining polymers at steady state*, these expressions have been used to calculate the bulk solution stresses from molecular conformations measured in single molecule experiments of DNA as discussed in previous work.[9] Here, we discuss the effect of neglecting HI and EV interactions in using the Giesekus stress tensor to estimate bulk solution stresses by comparing stresses calculated using the Kramers stress tensor in BD simulations in section 5.

4.3. Choice of Model Parameters. Our bead−spring model contains five parameters that are chosen in a systematic manner for DNA chains. We first consider the Kuhn step size (b_k) for dsDNA stained with YOYO-1 dye. At dye concentrations similar to those used in our experiments, b_k was found to increase by a factor of 1.32 from the native value of approximately 100 nm for unstained DNA in aqueous solution containing at least 10 mM monovalent salt.[44] Therefore, b_k is taken to be 0.132 μm. Next, we choose the quantity $N_{k,s}$ for a given level of discretization, and the number of springs $N_s = (N - 1)$ is then set by the constraint that the dimensional contour length $L = N_{k,s}N_s b_k$ is maintained at a particular value. For simulations of $L = 84$ μm DNA, we choose $N_s = 16$ and set $N_{k,s} = 40$. Only two parameters in the model remain: the bead radius (a) appearing in the RPY tensor and the excluded volume parameter (ν). We choose a and ν such that the BD simulations reproduce both the experimental center-of-mass diffusivities (D)[44] and relaxation times (τ) for DNA of contour length L. Longest polymer relaxation times are calculated in the same manner in experiment as in simulation as described in section 3. Center-of-mass chain trajectories were tracked to extract chain diffusivities (D) as described in previous work.[37]

The following set of parameters were then used for BD simulations of 84 μm DNA: $N_{k,s} = 40$, $N_s = 16$, $b_k = 0.132$ μm, $a = 0.101$ μm (or $h^* = 0.12$), and $\nu = 0.001$ μm^3. This parameter set yielded an average diffusivity of $D = 0.27$ μm^2/s in a 0.95 cP solvent and relaxation time τ of 282 s in a 300 cP buffer. Experimental values of chain diffusivity for 84 μm DNA, adjusted for changes in b_k due to YOYO-1 dye, are obtained by interpolation of data in previous work.[44] BD simulation results show that D is ≈15% higher than this (adjusted) experimental value. The relaxation time from simulation is 3.5% larger than the experimentally measured value[9] upon slight rescaling for polymer length.

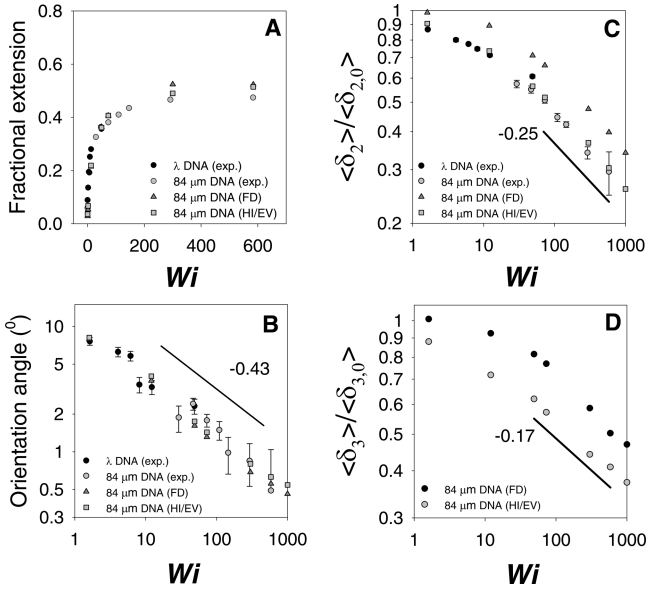

Figure 1. Experimental and BD simulation results of ensemble-averaged quantities of (a) fractional polymer extension, (b) orientation angle θ, (c) gradient direction polymer thickness $\delta_2/\langle\delta_{2,0}\rangle$, and (d) vorticity direction polymer thickness $\delta_3/\langle\delta_{3,0}\rangle$. Experimental results are shown for λ and 84 μm DNA. BD simulation results are shown for free-draining (FD) and HI/EV bead−spring models of 84 μm DNA.

5. Results and Discussion

The average fractional polymer extension in simple shear flow is shown in Figure 1a for experiment and for BD simulations of 84 μm DNA with results for λ-DNA (22 μm) included for comparison. Overall, good agreement between simulation and experiment is obtained for both free-draining bead−spring models and for models with intramolecular hydrodynamic interactions. For high flow strengths ($Wi = 300$ and 584), FD and HI/EV models slightly overpredict the average polymer extension, with results from FD DNA models slightly higher than HI/EV DNA average extensions. The same basic trends regarding the FD and HI/EV models were also observed by Jendrejack et al.[31] for simulations of DNA chains 126 μm in length in shear flow.

Figure 1b shows the average orientation angle θ as defined in eq 5 for DNA in shear flow as a function of Wi. Over the full (experimental) range of flow strengths ($Wi = 1.6-584$) for 22 and 84 μm DNA, the polymer orientation angle follows the scaling law $\theta \sim Wi^{-0.43}$. The thinning behavior of orientation angle calculated from BD simulation of 84 μm DNA with HI/EV follows the scaling $\theta \sim Wi^{-0.42}$ over the same Wi range, and the exponent becomes −0.40 between $Wi = 49-1000$. Previous light scattering studies provided measurements of the orientation angle of polymers in simple shear flow. However, because of technical limitations, the upper bound of flow strengths was generally limited to $Wi \approx 10-20$.[13,15,17] The birefringence extinction angle has also been measured in shear flow[45] for dimensionless flow strengths $Wi \leq 1$ with good agreement with model calculations. To our knowledge, this set of single molecule measurements of the polymer orientation angle via observations of DNA in the flow-gradient plane[9] is the first to provide experimental information regarding the thinning behavior of θ for high flow strengths. Polymer orientation angle has been previously studied

in shear flow using simulation techniques. Doyle et al.[11] and more recently Liu et al.[46] have calculated the polymer orientation angle using BD simulations of bead−rod chains, though neither quote a specific scaling law for θ as a function of Wi. Aust et al.[47] used molecular dynamics simulations of polymers obeying a finitely extensible nonlinear elastic (FENE) force law in shear flow to calculate the shear rate dependence of θ, finding $\theta \sim Wi^{-0.45}$ for high flow strengths. Finally, Cifre and de la Torre recently used BD simulation to calculate the orientational resistance parameter m, where $m = Wi \tan 2\theta$, as a function of flow strength for bead spring chains with HI and EV in shear flow. For bead−spring polymer chains with a nonlinear (FENE) force law, the orientational resistance parameter approximately follows a power law scaling with Wi for $Wi \gtrsim 100$, though the authors do not explicitly state a scaling law. Interestingly, for polymer chains with a linear force law, the authors find that the orientational resistance parameter is constant with flow strength for $Wi \gtrsim 100$.

The gradient direction polymer thickness (δ_2) is a microscopic conformational property that has direct influence on macroscopic solution behavior in shear flow. As discussed in section 4.2, the quantity δ_2 is directly related to the polymer contribution to the shear viscosity of a dilute solution of free-draining flexible polymers. Figure 1c shows a plot of ensemble-averaged δ_2 at steady state normalized to the equilibrium value at $Wi = 0$ for experiments and DNA simulation of 84 μm DNA. Good agreement between experiment and BD simulation of chains with HI/EV is shown. Although BD simulations of both FD and HI/EV chains show similar power law scalings of δ_2 as a function of Wi, results from FD chains overpredict the quantity $\langle\delta_2\rangle/\langle\delta_{2,0}\rangle$. Results from single molecule experiments of 84 μm DNA give the scaling $\langle\delta_2\rangle/\langle\delta_{2,0}\rangle \sim Wi^{-0.27}$ over the range $Wi = 73-584$. Results from BD simulation with HI/EV show $\langle\delta_2\rangle/\langle\delta_{2,0}\rangle \sim Wi^{-0.26}$ over the range $Wi = 73-1000$, which agrees well with scaling arguments based on a Graetz−Levecque dispersion layer model.[11,25] FD simulations show essentially the same thinning exponent as HI/EV results, and this observation was also noted by Jendrejack et al.[31] Finally, the thinning behavior of the vorticity direction polymer thickess from FD and HI/EV simulations is shown in Figure 1d. Although this quantity was not experimentally accessible using the flow apparatus in this study, we find that δ_3 scales with Wi as $\langle\delta_3\rangle/\langle\delta_{3,0}\rangle \sim Wi^{-0.17}$ over the range $Wi = 73-584$ from HI/EV simulations. Hur et al.[25] found $\langle\delta_3\rangle \sim Wi^{-0.20}$ for free-draining bead−rod chains consisting of 50 beads over a similar range of Wi. It seems counterintuitive that chains with excluded volume appear to be thinner in the vorticity direction according to Figure 1d. In fact, the magnitude of δ_3 is larger for chains with EV; however, when normalized to the equilibrium thickness, the quantity $\langle\delta_3\rangle/\langle\delta_{3,0}\rangle$ is larger for FD chains because $\langle\delta_3\rangle/\langle\delta_{3,0}\rangle$ is smaller. It should be noted that the size of the error bars on the data points in Figure 1d is smaller than the size of the data points.

Microscopic conformational information on polymers may be used to calculate macroscopic solution properties. Parts a and b of Figure 2 show the polymer contribution to the shear viscosity η^p and the first normal stress coefficient Ψ_1^p, respectively. In Figure 2a, results from BD simulation of chains with HI/EV agree well with experimental results for 84 μm DNA, while FD chains overpredict the quantity η^p/η_0^p. BD

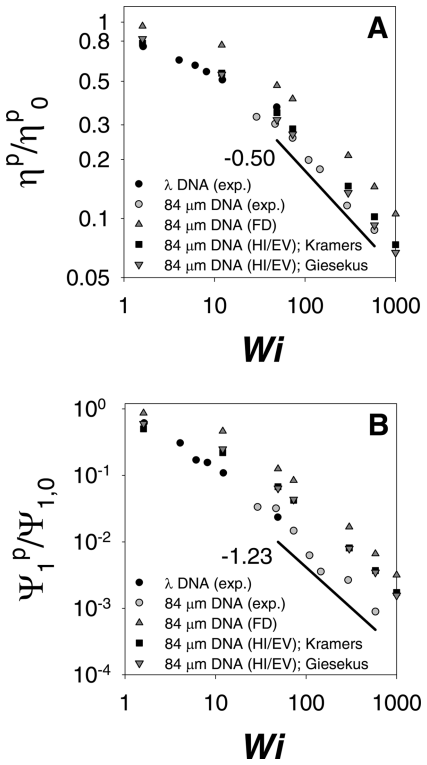

Figure 2. Macroscopic rheological properties: (a) polymer contribution to shear viscosity η^p and (b) first normal stress coefficient Ψ_1^p from BD simulation and single molecule experiments of DNA. η^p and Ψ_1^p from single molecule experiments and FD DNA models are calculated using the Giesekus stress tensor. η^p and Ψ_1^p for HI/EV models in BD simulations are calculated via the Kramers and Giesekus stress tensors.

simulation results for 84 μm DNA with HI/EV yield the scaling $\eta_p \sim Wi^{-0.52}$ for the Wi range 73−1000. This scaling law for η^p is obtained using the correct (HI-relevant) Kramers stress expression in eq 24 and the definition of η^p from eq 28. This shear thinning behavior agrees well with the experimental scaling law $\eta_p \sim Wi^{-0.53}$ obtained from single molecule measurements of 84 μm DNA in shear flow. The latter exponent regarding the decay of η^p was obtained using the Giesekus expression for the stress tensor and measurements of δ_2 from single molecule experiment.[9] Although eq 30 does not account for HI in the calculation of the stress, experimental results using the Giesekus stress tensor agree well with η^p calculated using Kramers stress from BD simulation results of 84 μm DNA with HI/EV. As shown in Figure 2a, shear viscosity calculated for DNA chains with HI/EV using the Giesekus stress tensor (which is not appropriate for chains with intramolecular HI) agree well with η_p results calculated with the Kramers stress expression. Furthermore, FD simulation results yield essentially the same scaling law for η^p calculated using the Giesekus stress tensor as HI/EV simulation results via the Kramers stress expression.

Figure 2b shows Ψ_1^p as a function of Wi. Results from BD simulations with HI/EV yield a scaling of $\Psi_1^p \sim Wi^{-1.23}$ over the Wi range 73−1000, again agreeing well with the scaling $\Psi_1^p \sim Wi^{-1.28}$ from single molecule experiment.[9] Furthermore, naive application of eqs 30 and 31 in the calculation of polymer stress for HI/EV chains gives $\eta_p \sim Wi^{-0.51}$ and $\Psi_1^p \sim Wi^{-1.24}$. It is clear that ignoring intramolecular HI in calculation of the polymer contribution to the stress does not lead to an

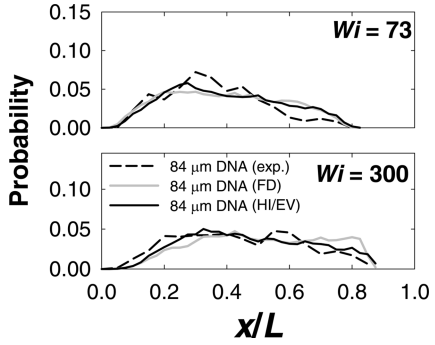

Figure 3. Histograms of polymer extension for 84 μm DNA in steady shear flow at $Wi = 73$ and 300. Results from single molecule experiment and BD simulation of FD and HI/EV chains are shown.

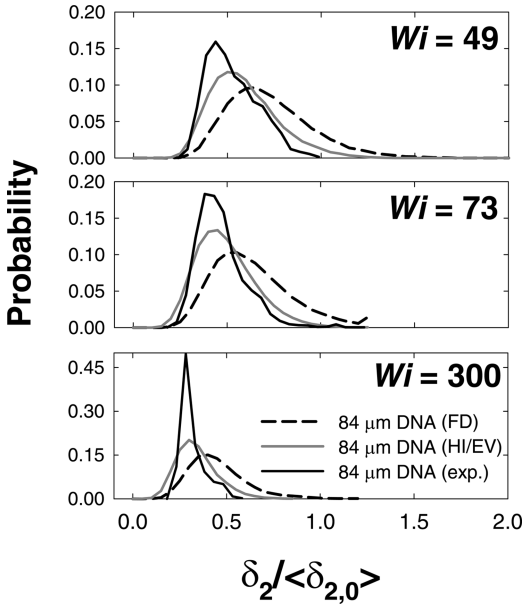

Figure 4. Histograms of gradient direction polymer thickness ($\delta_2/\langle\delta_{2,0}\rangle$) for 84 μm DNA in steady shear flow at $Wi = 49$, 73, and 300. Results from single molecule experiment and BD simulation of FD and HI/EV chains are shown.

appreciable change in the scaling law results for η^p and Ψ_1^p for 84 μm DNA. However, ignoring HI in stress calculations may lead to inaccurate results for larger DNA chains[20] as the role of conformation-dependent drag becomes increasingly important for polymers of greater length.

Figure 3 shows histograms of fractional polymer extension in the flow direction for 84 μm DNA in experiment and BD simulation. For $Wi = 73$ and 300, the probability of polymer extension is broadly distributed from very low to high fractional extensions. In shear flow, single polymers are continually undergoing large fluctuations in length as chains exhibit end-over-end tumbling motion. Results from both FD and HI/EV simulations agree well with experimental results regarding the probability of extension.

Histograms of the gradient direction polymer thickness normalized to equilibrium values ($\delta_2/\langle\delta_{2,0}\rangle$) for 84 μm DNA are plotted in Figure 4. The probability distributions of $\delta_2/\langle\delta_{2,0}\rangle$ show that polymer thickness gradually moves to smaller values of δ_2 upon increasing Wi. Reasonable agreement for the distribution of $\delta_2/\langle\delta_{2,0}\rangle$ between experiment and BD simulation of chains with HI/EV is obtained at $Wi = 49$ and 73. At $Wi = 300$, the

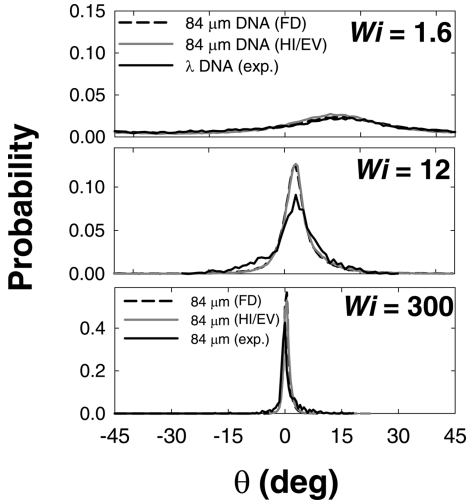

Figure 5. Histograms of orientation angle θ for λ and 84 μm DNA in steady shear flow at $Wi = 1.6$, 12, and 300. Results from single molecule experiment and BD simulation of FD and HI/EV chains are shown.

histogram of $\delta_2/\delta_{2,0}$ from experiment appears more peaked compared to results from BD simulations of DNA with HI/EV. Distributions of δ_2 from experiment and BD simulation appear to exhibit larger degrees of disagreement as Wi increases and δ_2 decreases and approaches the optical resolution limit of the microscope. The smallest measurable dimension (δ_{res}) using the optical setup described in Teixeira et al.[9] is $\approx$0.16 μm. Experimental data were analyzed to account for this inherent limitation of optical microscopy by deconvoluting the real image thickness from the resolution thickness limit.[9] Nonetheless, some disparity between experimental data and simulation results at high Wi is apparent in Figure 4. It should be noted that bead–spring chains also have a finite "thickness", and the size of an individual bead representing a chain subsection depends on discretization. In the present study, for example, the radius of gyration of a bead ($N_{k,s} = 40$) is $\approx$0.34 μm, suggesting that length resolution in bead–spring simulations may contribute to some inaccuracies in δ_2. At high Wi ($\gg$300), alternative polymer models may be more appropriate in resolving smaller scales in polymer configuration. A bead–rod model, for example, may provide finer length scale resolution.

Probability distributions of polymer orientation angle (θ) in steady shear are plotted in Figure 5. As the flow strength increases, polymer molecules are confined to increasingly thinner regions in the shear gradient direction and become more extended in the flow direction. As polymers align in the flow direction as Wi increases, the average orientation angle decreases but remains positive. Probability distributions of θ for λ-DNA and 84 μm DNA in experiment agree well with results from BD simulations of both FD and HI/EV chains over a wide range of Wi. At low Wi (=1.6), θ is broadly distributed. At high Wi values ($Wi = 300$), the distribution of θ is narrow and sharply peaked near zero. In this case, convection is strong and tends to align polymers in the flow direction, and thermal fluctuations quickly result in end-over-end tumbling or polymer restretching events. In the case of either tumbling or polymer restretch, the magnitude of the orientation angle (on average) remains small over the course of the event. The probability distribution of θ is asymmetric about $\theta = 0$, as it is clearly biased to positive values as

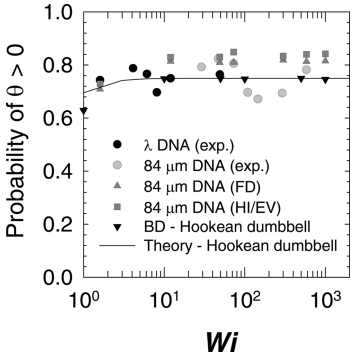

Figure 6. Fraction of probability distribution of orientation angle θ that occurs at positive values of angle as a function of *Wi*. Experimental and BD simulation results are shown. Solid line is analytical result for Hookean dumbbells from Woo and Shaqfeh.[48]

shown in Figure 5.

The probability of the polymer orientation angle occurring at positive values as a function of *Wi* is plotted in Figure 6. As noted in previous single molecule experimental work,[9] the fraction of time in which θ occurs at positive values is nearly constant at $\approx$0.75 for $Wi \geq 10$. Figure 6 shows the fraction of probability distribution for which $\theta > 0$ for single molecule experiments of DNA, BD simulations of multibead spring chains, and BD simulations of Hookean dumbbells. Clearly, the fraction of time representing positive polymer orientation angles is nearly constant over a wide range of *Wi* for both 22 and 84 μm DNA. BD simulations of multibead spring chains with and without HI/EV for 84 μm DNA show that the probability of positive θ is $\approx$0.8, slightly larger than for Hookean dumbbells. The solid line in Figure 6 represents theoretical predictions for Hookean dumbbels such that $\theta > 0$ and was given as an analytical result in Woo and Shaqfeh,[48] where the authors calculate the probability of linear dumbbells occurring in each quadrant of the flow-gradient in planar, two-dimensional mixed flows. The probabilities for dumbbell orientation in the (I) and (III) quadrants, P_{I} and P_{III}, are equal:

$$P_{\mathrm{I}} = \frac{1}{4} + \frac{1}{2\pi}\tan^{-1}\left(\frac{Wi}{\sqrt{1+Wi^2}}\right) \qquad (32)$$

Therefore, $2P_{\mathrm{I}}$ is equivalent to the total fraction of time a polymer spends with positive orientations to the total time for all orientations in flow, and for $Wi \gg 1$, $2P_{\mathrm{I}} \approx 0.75$. Differences between BD simulation results for Hookean dumbbells and theory at low *Wi* are due to differences in expression of relaxation times. In analytical calculations, the relaxation time for Hookean dumbbells is taken to be the characteristic time scale $\zeta/4H$, where H is the Hookean force law constant. However, longest relaxation times for Hookean dumbbells in BD simulations are calculated by extracting a time scale from a decaying exponential function fit to relaxation curves of mean-squared end-to-end extension of dumbbells. These values differ by $\approx$10%.

Complex dynamical behavior of flexible polymers in shear flow arises from the coupling between convection of the polymer in the flow direction and random fluctuations of polymer segments in the transverse, shear gradient direction. The first single molecule study of DNA in shear flow revealed large fluctuations in polymer extension in steady shear flow.[8] Recent work

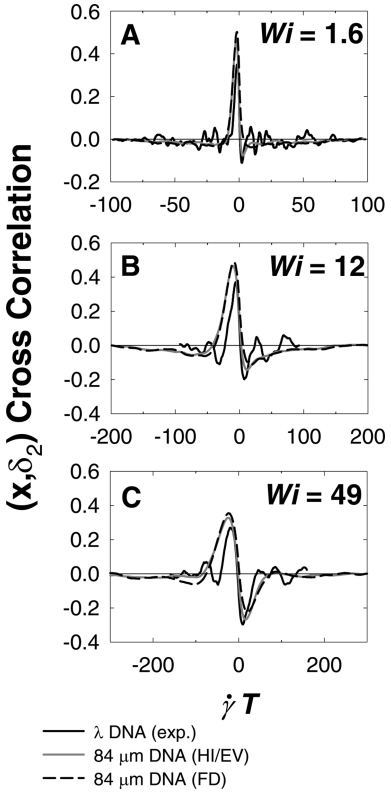

Figure 7. Cross-correlations of polymer extension x and gradient direction polymer thickness δ_2 in steady shear flow at $Wi = 1.6$, 12, and 49. Results from BD simulation of FD and HI/EV models of 84 μm DNA are shown with experimental results of λ DNA.

clearly showed unambiguous end-over-end polymer tumbling events.[9] These experimental studies and other BD simulations[25] reveal that although polymers are continually undergoing tumbling motion in flow, there is no deterministic cycle associated with polymer motion in terms of molecular extension. In short, there are no peaks in the PSD of polymer extension in steady shear flow. Therefore, no specific frequencies are being selected in the dynamic polymer motion in terms of the flow-direction polymer extension. However, the lack of apparent periodicity in polymer extension does not preclude a cyclical mechanism of polymer motion based on the interplay between two microscopic polymer conformational properties. Cross-correlations of deviations in polymer extension x and gradient direction polymer thickness δ_2 from their mean values are plotted vs fluid strain in Figure 7 for three different *Wi* values. Here, the cross-correlation is defined as

$$C_{x,\delta_2}(T) = \frac{\langle x'(t)\,\delta_2'(t+T)\rangle}{\sqrt{\langle x'^2(t)\rangle\langle \delta_2'^2(t)\rangle}} \qquad (33)$$

where a prime denotes deviations of a quantity from the mean value. As noted in previous work,[9,49,50] two features of the cross-correlation between x and δ_2 are clear as shown in Figure 7: large peaks at negative strain lags and deep valleys at positive strain. Peaks at negative strain lags suggest that positive deviations in polymer extension from its mean value are correlated with previous positive fluctuations in δ_2. In other words, thickening of δ_2 is on average *followed by extension of the polymer to values larger than its mean value*. A thermal fluctuation leading to an increase in δ_2 will

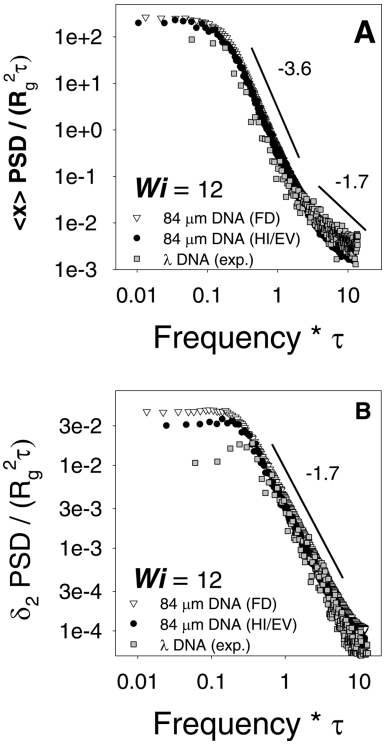

Figure 8. Power spectral density (PSD) of (a) polymer extension and (b) gradient direction polymer thickness δ_2 in steady shear flow at $Wi = 12$. Experimental data for λ DNA are compared with BD simulations of DNA using both FD and HI/EV models.

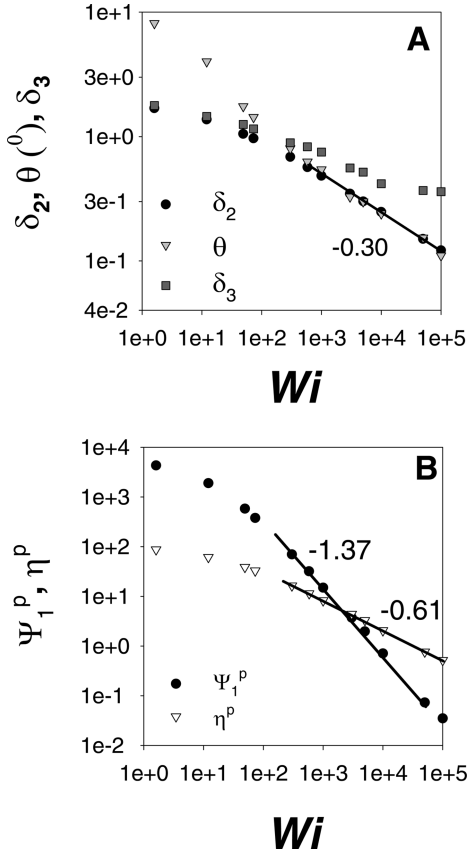

Figure 9. High Wi power law scalings of (a) microscopic conformational properties and (b) macroscopic solution rheological properties of 84 μm DNA in steady shear flow. Results are plotted from BD simulations of DNA with HI/EV.

cause a corresponding increase in polymer extension as the velocity difference across the chain becomes larger, and polymer segments are advected relative to one another in the flow direction. Also, polymer recoiling events following thinning in δ_2 due to polymer alignment in the flow direction also contributes to peaks at negative strain lag. Conversely, valleys at positive strain lag illustrate that positive deviations in polymer extension are on average *followed by negative fluctuations in* δ_2. A polymer may only stretch a finite amount in the flow direction due to its finite extensibility, and the subsequent stiffening of the entropic spring upon extension in the flow direction causes δ_2 to decrease. Valleys at positive strain lag may also be attributed to thickening of δ_2 following polymer recoiling in the flow direction. Cross-correlations are shown in Figure 7 for $Wi =$ 1.6, 12, and 49 for λ-DNA (22 μm) in experiment and 84 μm DNA from BD simulation. Similar trends in $C_{x,\delta_2}(T)$ are observed for both 22 and 84 μm DNA. This observation suggests that the cyclical polymer behavior in steady shear flow results from a phenomenon that affects DNA regardless of length. In short, for chains with a nonlinear entropic restoring force law, a coupling between chain advection due to flow and polymer segment diffusion is responsible for trends in the cross-correlation of x and δ_2. In polymer chains with a linear (Hookean) entropic force law, thinning of the polymer in the shear gradient direction is uncoupled with polymer stretch due to advection because the chain is infinitely extensible.[49,50] Hence, valleys in $C_{x,\delta_2}(T)$ are absent for chains with a linear force law.

PSDs of polymer extension are shown in Figure 8a for 22 μm DNA in experiment and for 84 μm DNA from BD simulation results. All PSDs in Figure 8a show the same qualitative shape and the same quantitative power-law decay constants. A plateau at low frequencies ($f\tau \ll 1$) is followed by a sharp decay observing the power law $P(f) \sim (f\tau)^{-3.6}$. Finally, a third frequency regime is evident at high frequencies where $P(f) \sim (f\tau)^{-1.7}$.[8,25] Physically, power occurring at low frequencies corresponds to polymer motion caused by convection. Furthermore, power at high frequencies corresponds to polymer motion arising from short time scale Brownian motion, and power decay in intermediate frequency regimes results from a balance between chain motion caused by convection but driven by thermal fluctuations in the shear gradient direction.[25] No distinct peaks are present in the PSDs of polymer extension as noted by previous work.[8,25] Figure 8b shows PSDs of gradient direction polymer thickness δ_2 at $Wi = 12$ for 22 and 84 μm DNA in shear flow. A plateau at low frequencies is followed by a power law decay of $P(f) \sim (f\tau)^{-1.7}$. As expected, the behavior of δ_2 at high frequencies is governed by only diffusion in the shear gradient plane, as indicated by the power law decay constant.

Figure 9a shows results from BD simulation of 84 μm DNA with intramolecular HI and EV at high Wi. The polymer gradient direction thickness δ_2 scales with Wi as $\delta_2 \sim Wi^{-0.30}$ over the Wi range 584−10^5, slightly steeper than noted in Figure 1c over the Wi range 73−1000. Similar behavior was noted by Jendrejack et al.[31] for high Wi regimes. Furthermore, orientation angle θ begins to scale with Wi as $\theta \sim Wi^{-0.34}$, nearly the same power law decay as exhibited by δ_2. For free-draining chains, Woo et al.[48] predicted that the polymer orientation angle $\theta \sim \delta_2$ for $Wi \gg 1$. Therefore, θ should scale similarly with Wi as δ_2 for free-draining chains at high Wi. Finally, δ_3 begins to plateau above $Wi \approx 10^4$, presumably as excluded volume interactions between

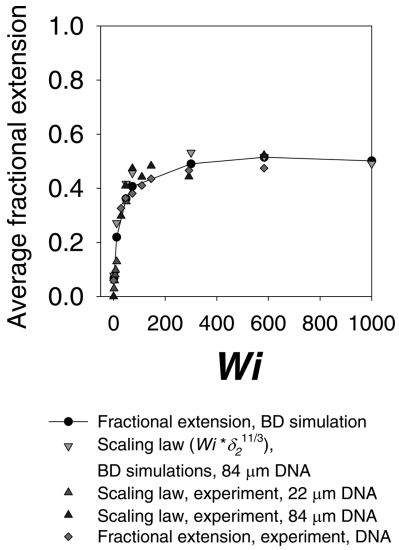

Figure 10. Scaling law analysis for average polymer extension $\langle x \rangle$ in steady shear flow. Prediction of average fractional extension from scaling analysis is compared with experimental results for lambda and 84 μm DNA and with BD simulation results for 84 μm DNA.

beads play a role in vorticity thickness thinning. Figure 9b shows plots of the polymer contribution to the first normal stress coefficient Ψ_1^p and shear viscosity η^p as calculated from the Kramers stress tensor. Again, at high Wi values $Wi \geq 10^3$, both Ψ_1^p and η^p decay more rapidly with Wi than for the lower Wi range shown in Figure 2. Both exponents in the power-law decay approach the "classical" Graetz−Leveque results describing the balance between convection and diffusion which predict $\Psi_1^p \sim Wi^{-4/3}$ and $\eta^p \sim Wi^{-2/3}$.[11,31]

Finally, we apply scaling law analysis to describe the average extension of free polymer molecules in steady shear flow. In short, the average distance a polymer chain may extend $\langle x \rangle$ during the stretch phase of the dynamical cycle scales as the product of stretching rate with average duration of a stretching event. The stretching rate is given by the product of polymer gradient direction thickness δ_2 and the shear rate $\dot{\gamma}$. As discussed above and in previous work,[9] a polymer chain may remain stretched and nearly aligned with the flow axis such that $\theta \approx 0$ until a Brownian fluctuation leads to a negative orientation angle $\theta < 0$ and subsequent polymer tumbling. The time scale for polymer angle flipping is set by a diffusive process such that $t^{flip} \propto \langle \delta_2 \rangle^2 / D(\delta_2)$.[9] Therefore, average polymer stretch in unbounded shear flow scales as

$$\langle x \rangle \propto Wi \langle \delta_2 \rangle \frac{\langle \delta_2 \rangle^2}{D(\delta_2)} \propto Wi \langle \delta_2 \rangle^{11/3} \qquad (34)$$

This simple scaling law analysis predicts average polymer extension in steady shear flow for experiment and simulation results reasonably well over 3 orders of magnitude in Wi as shown in Figure 10.

6. Conclusion

In this work, we compare BD simulation results for 84 μm DNA to single molecule experimental results obtained using a novel flow apparatus that allows for flow-gradient plane observation of DNA dynamics in shear flow. Results from BD simulations employing both free-draining and HI/EV models with interbead excluded volume interactions are discussed. Good agreement between simulation and experiment is obtained for ensemble average measurements of polymer extension, orientation angle, and gradient direction polymer thickness over a wide range of Wi in steady shear flow. Furthermore, the polymer contribution to shear viscosity η^p calculated via the Giesekus expression from single molecule measurements of polymer conformation agrees well with η^p calculated from BD simulations of HI/EV chains using the Kramers stress tensor. However, results from BD simulations of FD chains in terms of η^p/η_0^p calculated from the Giesekus stress tensor slightly disagree with experiment and HI/EV chains from simulation, though the correct power law decay is recovered. BD simulations of both FD and HI/EV chains give similar power law decays as experimentally calculated $\Psi_1^p/\Psi_{1,0}$. Histograms of polymer extension and orientation angle for 84 μm DNA from BD simulation agree well with experimental measurements. Cross-correlations of polymer extension with δ_2 from experiment and simulation show large peaks and valleys at negative and positive strain lag, respectively for $Wi > 1$. Features in the cross-correlations of x and δ_2 are explained on a physical basis and arise from polymer motion controlled by a coupling between convection and diffusion and the finite extensibility of a polymer chain. Power law decays of PSDs of polymer extension and δ_2 from BD simulation quantitatively agree with experimental results and previous experimental findings. High Wi scaling of polymer conformational properties δ_2 and θ and macroscopic observables such as Ψ_1^p and η^p agree well with classical scaling arguments and rheological measurements on dilute polymer solutions. Finally, our observations suggest that inclusion of intramolecular HI/EV does not qualitatively change the dynamical behavior of DNA up to $\approx$84 μm in length in shear flow.

Acknowledgment. We thank H. Babcock for help with construction of the experimental apparatus and M. Gallo and E. Chan at U.S. Genomics for providing DNA samples. This work was supported, in part, by grants from the Materials Research Science and Engineering Center Program of the National Science Foundation (NSF) under DMR-0213618 and DMR-9808677, the Air Force Office of Scientific Research, and the NSF. C. M. Schroeder was supported by NSF graduate and Lieberman fellowships.

References and Notes

(1) Larson, R. G. *The Structure and Rheology of Complex Fluids*; Oxford University Press: New York, 1999.
(2) Öttinger, H. C. *Stochastic Processes in Polymeric Fluids*; Springer: Berlin, 1996.
(3) De Gennes, P. G. *J. Chem. Phys.* **1974**, *60*, 5030.
(4) Batchelor, G. K. *An Introduction to Fluid Dynamics*; Cambridge University Press: Cambridge, 2000.
(5) Fuller, G. G.; Leal, L. G. *Rheol. Acta* **1980**, *19*, 580.
(6) Babcock, H. P.; Teixeira, R. E.; Hur, J. S.; Shaqfeh, E. S. G.; Chu, S. *Macromolecules* **2003**, *36*, 4544.
(7) Perkins, T. T.; Smith, D. E.; Chu, S. *Science* **1997**, *276*, 2016.
(8) Smith, D. E.; Babcock, H. P.; Chu, S. *Science* **1999**, *283*, 1724.
(9) Teixeira, R. E.; Babcock, H. B.; Shaqfeh, E. S. G.; Chu, S. *Macromolecules*, submitted for publication.
(10) Liu, T. W *J. Chem. Phys.* **1989**, *90*, 5826.
(11) Doyle, P. S.; Shaqfeh, E. S. G.; Gast, A. P. *J. Fluid Mech.* **1997**, *334*, 251.
(12) Cottrell, F. R.; Merrill, E. W.; Smith, K. A. *J. Polym. Sci., Polym. Phys.* **1969**, *7*, 1415.

(13) Link, A.; Springer, J. *Macromolecules* **1993**, *26*, 464.
(14) Zisenis, M.; Springer, J. *Polymer* **1994**, *35*, 3156.
(15) Lee, E. C.; Solomon, M. J.; Muller, S. J. *Macromolecules* **1997**, *30*, 7313.
(16) Lee, E. C.; Muller, S. J. *Macromolecules* **1999**, *32*, 3295.
(17) Li, L.; Larson, R. G. *Macromolecules* **2000**, *33*, 1411.
(18) Perkins, T. T.; Smith, D. E.; Larson, R. G.; Chu, S. *Science* **1995**, *268*, 83.
(19) Smith, D. E.; Chu, S. *Science* **1998**, *281*, 1335.
(20) Schroeder, C. M.; Babcock, H. P.; Shaqfeh, E. S. G.; Chu, S. *Science* **2003**, *301*, 1515.
(21) Babcock, H. P.; Smith, D. E.; Hur, J. S.; Shaqfeh, E. S. G.; Chu, S. *Phys. Rev. Lett.* **2000**, *85*, 2018.
(22) Zylka, W.; Öttinger, H. C. *J. Chem. Phys.* **1988**, *90*, 474.
(23) Bird, R. B.; Curtiss, C. F.; Armstrong, R. C.; Hassager, O. *Dynamics of Polymeric Liquids*, 2nd ed.; Wiley: New York, 1987; Vol. 2.
(24) Wedgewood, L. E. *J. Non-Newtonian Fluid Mech.* **1989**, *31*, 127.
(25) Hur, J. S.; Shaqfeh, E. S. G.; Larson, R. G. *J. Rheol.* **2000**, *44*, 713.
(26) Marko, J. F.; Siggia, E. D. *Macromolecules* **1995**, *28*, 8759.
(27) Hur, J. S.; Shaqfeh, E. S. G.; Babcock, H. P.; Smith, D. E.; Chu, S. *J. Rheol.* **2001**, *45*, 421.
(28) Lyulin, A. V.; Adolf, D. B.; Davies, G. R. *J. Chem. Phys.* **1999**, *111*, 758.
(29) Kröger, M.; Alba-Perez, A.; Laso, M.; Öttinger, H. C. *J. Chem. Phys.* **2000**, *113*, 4767.
(30) Jendrejack, R. M.; Graham, M. D.; de Pablo, J. J. *J. Chem. Phys.* **2000**, *113*, 2894.
(31) Jendrejack, R. M.; de Pablo, J. J.; Graham, M. D. *J. Chem. Phys.* **2002**, *116*, 7752.
(32) Cascales, J. J. L.; de la Torre, J. G. *Polymer* **1991**, *32*, 3359.
(33) Cascales, J. J. L.; Díaz, F. G.; de la Torre, J. G. *Polymer* **1995**, *36*, 345.
(34) Cascales, J. J. L.; Navarro, S.; de la Torre, J. G. *Macromolecules* **1992**, *25*, 3574.
(35) Cifre, J. G. H.; de la Torre, J. G. *Macromol. Theory Simul.* **2004**, *13*, 273.
(36) Hsieh, C. C.; Li, L.; Larson, R. G. *J. Non-Newtonian Fluid Mech.* **2003**, *113*, 147.
(37) Schroeder, C. M.; Shaqfeh, E. S. G.; Chu, S. *Macromolecules* **2004**, *37*, 9242.
(38) Press, W. H.; et al. *Numerical Recipes in Fortran 77*; Cambridge University Press: Cambridge, 1997.
(39) Ermak, D. L.; McCammon, J. A. *J. Chem. Phys.* **1978**, *69*, 1352.
(40) Russel, W. B.; Saville, D. A.; Schowalter, W. R. *Colloidal Dispersions*; Cambridge University Press: New York, 1989.
(41) Rotne, J.; Prager, S. *J. Chem. Phys.* **1969**, *50*, 4831.
(42) Somasi, M.; Khomami, B.; Woo, N. J.; Hur, J. S.; Shaqfeh, E. S. G. *J. Non-Newtonian Fluid Mech.* **2002**, *108*, 227.
(43) Doi, M.; Edwards, S. F. *The Theory of Polymer Dynamics*; Clarendon: Oxford, 1986.
(44) Smith, D. E.; Perkins, T. T.; Chu, S. *Macromolecules* **1996**, *29*, 1372.
(45) Bossart, J.; Öttinger, H. C. *Macromolecules* **1997**, *30*, 5527.
(46) Liu, S.; Ashok, M.; Muthukumar, M. *Polymer* **2004**, *45*, 1383.
(47) Aust, C.; Kröger, M.; Hess, S. *Macromolecules* **1999**, *32*, 5660.
(48) Woo, N. J.; Shaqfeh, E. S. G. *J. Chem. Phys.* **2003**, *119*, 2908.
(49) Chopra, M.; Larson, R. G. *J. Rheol.* **2002**, *46*, 831.
(50) Woo, N. J.; Shaqfeh, E. S. G.; Khomami, B. *J. Rheol.* **2004**, *48*, 299.

MA0480796